5-3-2017

Using Phase for Radar Scatterer Classification

Linda J. Moore
Air Force Research Laboratory

Brian D. Rigling
Wright State University

Robert Penno
University of Dayton, rpenno1@udayton.edu

Edmund G. Zelnio
Air Force Research Laboratory

Using phase for radar scatterer classification

Linda J. Moore[a,b], Brian D. Rigling[c], Robert P. Penno[b], and Edmund G. Zelnio[a]

[a]Air Force Research Laboratory Sensors Directorate, 2241 Avionics Circle, WPAFB, OH 45433-7321
[b]University of Dayton, 300 College Park, Dayton, OH, 45469-0232
[c]Wright State University, 3640 Colonel Glenn Highway, Dayton, OH, 45435-0001

ABSTRACT

Traditional synthetic aperture radar (SAR) systems tend to discard phase information of formed complex radar imagery prior to automatic target recognition (ATR). This practice has historically been driven by available hardware storage, processing capabilities, and data link capacity. Recent advances in high performance computing (HPC) have enabled extremely dense storage and processing solutions. Therefore, previous motives for discarding radar phase information in ATR applications have been mitigated. First, we characterize the value of phase in one-dimensional (1-D) radar range profiles with respect to the ability to correctly estimate target features, which are currently employed in ATR algorithms for target discrimination. These features correspond to physical characteristics of targets through radio frequency (RF) scattering phenomenology. Physics-based electromagnetic scattering models developed from the geometrical theory of diffraction are utilized for the information analysis presented here. Information is quantified by the error of target parameter estimates from noisy radar signals when phase is either retained or discarded. Operating conditions (OCs) of signal-to-noise ratio (SNR) and bandwidth are considered. Second, we investigate the value of phase in 1-D radar returns with respect to the ability to correctly classify canonical targets. Classification performance is evaluated via logistic regression for three targets (sphere, plate, tophat). Phase information is demonstrated to improve radar target classification rates, particularly at low SNRs and low bandwidths.

Keywords: radar range profile, phase information, magnitude profile, classification, automatic target recognition, feature extraction, Cramér-Rao lower bound, error analysis

1. INTRODUCTION

In legacy radar applications, to reduce storage and simplify exploitation, only magnitude data is used by target classification algorithms. The increase in available data processing speed and storage capability, coupled with the decrease in size and cost of the corresponding hardware, makes retaining phase information reasonable from a data management perspective. Therefore, it is important to revisit the impact of phase in radar automatic target recognition (ATR) applications, as any possible retention of usable information is imperative for continued improvement of ATR performance. An additional argument in the past for discarding phase information was that the phase present in synthetic aperture radar (SAR) imagery was largely due to diffuse scattering, or scattering from the naturally occurring environment, as opposed to scattering from man-made objects.[1,2] Further, the usage of low resolution SAR sensors resulted in many scatterers per resolution cell and the phase within a resolution cell was subsequently believed to be uniformly distributed between π and $-\pi$.[1] Due to the current availability of high resolution sensors, the phase within a resolution cell is thought to be dominated by a single scatterer and is no longer randomly distributed; thus, phase can be exploited for a number of purposes including target identification.[1] In this manuscript, we first show that phase enables improved estimation of canonical target features from noisy received radar signals. We then demonstrate that use of phase information within radar signals results in improved classification of canonical scatterers compared to classification when phase is discarded.

This manuscript is organized as follows. Section 2 provides motivation for the research pursued in this effort. Section 3 offers a summary of previous research relating to the work presented here. Section 4 describes the electromagnetic physical scattering model, based on the geometrical theory of diffraction, employed for estimation of canonical target features from 1-D radar range profiles. Section 5 demonstrates feature estimation performance when phase is excluded compared to feature estimation when phase is retained; these results are then used to assist in predicting classification performance for canonical targets. Section 6 describes electromagnetic physical scattering models employed for target classification

Further author information: (E-mail: linda.moore.10@us.af.mil)

Algorithms for Synthetic Aperture Radar Imagery XXIV, edited by Edmund Zelnio, Frederick D. Garber,
Proc. of SPIE Vol. 10201, 102010J · © 2017 SPIE · CCC code: 0277-786X/17/$18 · doi: 10.1117/12.2267832

studies given 1-D radar signatures. The scattering models in Section 6 are extensions of the model from Section 4 and include additional degrees of freedom, such as the ability to specify length, height and radius of the canonical scattering objects. Section 7 describes logistic regression for multinomial classification. Section 8 details the process by which target features were defined and generated for the classification studies presented in this manuscript. Section 9 provides classification results for canonical targets which demonstrate that phase information enables improved classification performance, particularly at low signal-to-noise ratios (SNRs) and low bandwidths. Finally, Sections 10 and 11 offer conclusions and suggestions for future work, respectively.

The following notational conventions are employed throughout this paper. Vectors are denoted by uppercase or lowercase letters with an arrow or tilde placed above the letter, e.g., $\vec{s}(\cdot)$ or $\tilde{S}(\cdot)$. In general, vectors describing frequency-domain data are denoted by uppercase letters, e.g., $\vec{S}(\cdot)$, whereas vectors containing image-domain data are represented by lowercase letters, e.g., $\vec{s}(\cdot)$. One exception to this is the vector describing noise present in collected radar frequency-domain data, which is designated by $\vec{n}(\cdot)$. In this case, the arguments of the vector function will denote if the noise is in the frequency or image domain. Matrices are represented by letters in bold font, e.g., $\mathbf{Q}$. Elements of vectors or matrices are indicated by lowercase subscripts, e.g., $\vec{S}_i(\cdot)$ or $\mathbf{Q}_{v,w}$. If the length of a particular vector is given by an uppercase letter, e.g., K, then the subscript used to designate individual elements of the vector will be the corresponding lowercase letter, e.g., k. Scalars may be signified by either uppercase or lowercase letters, but will not be displayed in bold font and will not have symbols or accents placed above the letter.

2. MOTIVATION

ATR algorithms aim to achieve what humans achieve effortlessly. It has been noted that humans seem to have an inherent ability to recognize an object independent of its translation, rotations, or perspective viewing [3] and also have other invariant recognition capabilities to changes in brightness, color, and to the partial occlusion of an object. [3] However, it is currently unknown exactly how humans accomplish this seemingly automatic and reliable object recognition. ATR algorithms hope to achieve this same level of success and ease of distinguishing targets from one another. One of the major difficulties, for example, is that in an electromagnetic sense, a target may look drastically different when observed from various angles due to the way the energy reacts to the object's shape. Here we focus on quantifying the decrease in achievable target characterization when phase information is discarded.

The distinct and complex challenges facing an ATR system serve as a specific motivation for this work. ATR algorithms aim to correctly classify an unknown target of interest given some information collected on the target by a sensor. Here, the sensor is assumed to be a radar system. The ability to successfully identify an unknown target from data collected by a sensor depends on a number of conditions. Some of these conditions can be controlled through ATR system design, such as sensor parameters or choice of classifier, while others cannot, such as target motion and environmental contributors. [4–7] Since real world operating conditions (OCs) cannot be explicitly influenced, the best an ATR system can hope to achieve is the optimal extraction of all available relevant information from a measured signal on a target of interest. This task, however, is not straightforward and many strategies exist for information extraction and exploitation from collected target data. A commonly employed approach, for example, is to extract features from measured target responses. These features correspond to physical scattering characteristics of the target. The goal of these techniques is to capture the most pertinent target information available in the data to maximize target separability within an ATR system. Often, determining the usefulness of particular features embedded in measured signals is achieved through extensive testing and evaluation involving large data sets (some measured, some synthetically generated) and particular ATR algorithms or target classifiers. This methodology lends itself to a considerable use of resources, including the time and cost of both the data collection and the subsequent testing phase. In addition, some limitations on the accuracy of ATR system performance predictions are naturally present given the lack of generality presumed.

Even assuming a target's response is completely known, an ATR algorithm is still presented with a great challenge when it must distinguish between a particular target and others that look similar in an electromagnetic sense. It has been noted that improvements in sensor data would naturally arise as a result of a thorough understanding of the limiting factors in performance.[5] This research aims to identify the limiting factors in performance when phase information is discarded prior to target classification. Further, we seek to predict the degradation in classification performance if phase is excluded without having to perform extensive testing over a wide range of potential ATR algorithms.

From the existence of target information in the real world, to the capture of some of that information through the measurement of a signal, to the processing of collected data for the purposes of target classification, relevant information

for ATR is changed or lost as a result of many differing nonlinear systems or channels through which the information passes. Currently, a lack of fundamental understanding exists as to how a single block in the information transfer chain, representing a single way an information-encoded signal is transformed in a nonlinear fashion, ultimately affects classification performance. Given the limitations and expenses of empirical classification performance evaluation, we seek to obtain a theoretical foundation for the prediction of ATR system performance with respect to one such block in a typical information transfer chain that involves discarding phase information. Phase information has been historically discarded after radar image formation and prior to target classification due to data storage and processing constraints. Advances in high performance computing (HPC) have resulted in the availability of increased processing and storage capabilities at reduced size, weight and power for lower costs. With previous data management-related barriers now removed, we seek to quantify the impact of information in radar phase as it relates to the ability to perform reliable target classification or identification.

3. BACKGROUND

A commonly employed approach to ATR is to extract features from measured target responses.[8] These features often correspond to physical scattering characteristics of the target.[9] Several methods for feature extraction exist.[8–23] Some feature extraction algorithms have exploited information in complex radar data.[24–27] The goal of any feature extraction technique is to capture the most important components of the data, from a target uniqueness perspective, that will allow discrimination of a particular target from other targets that might also be observed by the sensor. The following literature review demonstrates a growing interest in the radar community to evaluate, quantify and perhaps alter conventional thinking regarding the retention and exploitation of phase information. This research seeks to lay a theoretical framework built upon the evaluation of canonical scattering phenomenology such that additional degrees of complexity may be added over time in order to thoroughly understand and quantify the impact of phase on radar exploitation.

Previous work has addressed the information content of radio frequency (RF) phase measurements from a variety of viewpoints. Some research addressed the issue of the estimation of target features from radar data when phase was discarded. In one example, the author acknowledged ambiguity in the radar community over the usefulness of phase information.[28] In particular, a definition of "functional" resolution was proposed over the traditional definition of resolution. It was argued this functional resolution measure offers additional practicality over traditionally employed definitions because it not only requires that two nearby scatterers are indeed detected via two peaks within radar imagery, but also that accurate estimations of the target locations are possible. The author showed that inclusion of phase information improved the functional resolution by a factor of two. Additional work by this author argued that man-made objects exhibit dispersive scattering and that exploitation of complex imagery is necessary to extract all relevant information about detected targets.[29] Building upon that work,[29] additional research demonstrated the recognition of dispersive scattering components in complex SAR imagery.[30] These dispersive features capture the phenomenology of the dominant scatterers of complex targets. In other work,[31] phase information of 1-D high range resolution (HRR) profiles was investigated through direct examination of a representative HRR model for stationary targets. This model contained target parameters of position and complex-valued scattering coefficient, but did not contain an additional parameter, α, addressed in this manuscript, which represents the target scattering geometry or curvature. In addition, an electronic warfare application motivated the study of phase information impact on estimation of pulse time of arrival of detected RF waveforms.[32] Waveform parameter estimates are commonly performed using pulse envelopes, effectively discarding phase information. The cited work showed that retention of phase information indeed improved accuracy of pulse time of arrival estimates, which are used by electronic warfare receivers for waveform classification and threat identification.

In other related works,[1,2] the historical issue of random phase in SAR imagery was addressed given the use of low resolution SAR sensors. High resolution sensors, especially those operating over urban environments where the large presence of man-made objects promotes majority specular scattering instead of diffuse scattering, remove the historical assumption that phase is uniformly distributed and therefore, uninformative.[1,2] These works developed statistical models for characterizing the probability distributions of non-uniform phase within high resolution SAR imagery so that it can be further exploited to achieve goals such as target classification.

In early work on identification of complex targets with low frequency radar, it was found that inclusion of phase information reduced the probability of misclassification compared to performance observed when only magnitude data was available.[33] In this case, a priori knowledge of the target's aspect angle was assumed. In related work,[34] the utility of phase in radar range profiles for target recognition was investigated by computing the correlations between range profiles

with different aspect angles when phase is included or discarded. The authors concluded that phase contains valuable information that may be applicable to radar target recognition problems. In other relevant works, [35,36] complex and real HRR profiles were used for radar target recognition where features were determined using principal component analysis. These works showed reduced error rates in target recognition experimentation; however, the authors acknowledged that more work is required as many existing radar feature extraction algorithms simply will not accept complex data as inputs. In another published work,[37] features were extracted from complex and real HRR profiles for the purposes of target recognition. A minimal Euclidean distance classifier was used to demonstrate that retention of phase results in improved target recognition rates.

In a ground penetrating radar (GPR) application, novel signal processing techniques were proposed that enable extraction of both amplitude and phase information for buried objects. [38,39] The output signals are suitable for use in target classification algorithms. The authors were motivated by the belief that amplitudes of measured radar signals allow for detection and localization of a buried target while phase information will enable discrimination among targets.

In other research of interest,[40] a series of studies were performed to measure the impact of phase in SAR imagery with respect to classification performance. Specifically, a number of divergence functions were considered, to include Bhattacharyya distance, Jeffries–Matusita distance, Kullback–Leibler distance, and the Kolmogorov-Smirnov test. In all applications of these probability distribution separation measures to a particular set of complex SAR data, the inclusion of phase information resulted in larger pattern separations than when only the magnitude data was used. In another work, [27] target scattering features were extracted from complex and magnitude SAR imagery via the Hilbert-Huang transform. Improvements in classification accuracy for a particular data set were demonstrated when radar phase was employed compared to the use of magnitude SAR imagery.

In other works investigating radar phase,[41,42] information content of complex-valued radar target signatures as a whole were considered in the context of efficient target database development for ATR applications. A collection of 1-D radar range profiles of a stationary target from similar aspect angles were considered to be independent samples of a random process. Eigenvalue decomposition was performed on the covariance matrix representing this signal space in order to identify the information content. Information theoretic principles, namely mutual information, were used to determine similarity between targets using the described complex-valued signal space.

In related works by one author of this manuscript,[43,44] the estimation of target parameters – location, scattering coefficient, and frequency dependence (α) – was performed given 1-D radar range profiles and 2-D SAR imagery with phase either retained or discarded. In those works, the target was assumed to be stationary, and the scattering was assumed to be real-valued and therefore representative of a perfect electrical conductor (PEC). When phase was retained, the Cramér-Rao lower bound (CRLB), previously derived, was validated against numeric estimation of target parameters using maximum likelihood estimation (MLE). For the case in which phase was discarded, target parameter estimation was performed using a least squares estimation (LSE) technique. The cited works demonstrated that inclusion of phase in target parameter estimation improves the accuracy of the estimates. Building upon that research, phase information in 1-D radar range profiles for stationary targets was further explored by the authors of this manuscript. [45] Target scattering was assumed to be complex-valued, thus removing the PEC assumption, and a novel analytical expression for the CRLB was derived for estimation of target parameters when phase is excluded from 1-D range profiles. [45] Target parameter estimation error was initially presented in the cited work as a function of SNR for a single operating bandwidth at X-band; here, we provide feature estimation error results for multiple bandwidths. Target parameter estimation was also performed via numeric simulation using MLE and LSE to validate analytical CRLB expressions when phase was included and excluded, respectively.[45] The authors of this manuscript later derived a generalized CRLB expression for 2-D magnitude SAR imagery, of which the CRLB for 1-D radar range profiles was shown to be a special case.[46] In addition, the authors offered an analysis of phase impact on target feature extraction from 1-D and 2-D SAR imagery given a range of realistic OCs, including various bandwidths, SNRs and aperture extents (for 2-D SAR phase histories).[46] CRLB studies investigating the impact of radar phase on target feature extraction demonstrated improved feature estimation accuracy when phase was retained for both 1-D radar range profiles[45,46] and 2-D SAR imagery.[46] The impact of phase on target parameter estimation, however, was not equal for all target parameters.

4. PHYSICAL SCATTERING MODEL FOR FEATURE ESTIMATION

For target feature extraction, we employ an electromagnetic scattering model developed from the geometrical theory of diffraction[47] to represent the radar phase history for a high range resolution, real aperture radar as an aggregate of scattering

Table 1: α Values for Canonical Scatterers

α	Scattering Geometries
1	flat plate at broadside; dihedral; trihedral
0.5	singly curved surface reflection; tophat
0	point; sphere; straight edge specular
-0.5	edge diffraction
-1	corner diffraction

returns from P canonical targets given N frequency samples, $f_n|_{n=1,...,N}$, in Hertz,[48]

$$S(f_n) = \sum_{p=1}^{P} A_p \left(\frac{jf_n}{f_c}\right)^{\alpha_p} \exp\left(\frac{-j4\pi f_n x_p}{c}\right), \tag{1}$$

where c is the propagation speed in meters/second, and f_c is the center frequency in Hertz. The measured 1-D radar phase history from a single transmitted pulse given N frequency samples,

$$\Psi(f_n) = S(f_n) + n(f_n), \quad n = 1, ..., N, \tag{2}$$

is corrupted by circular white Gaussian noise, $n(f_n)$, with variance σ^2. Therefore, the real and imaginary parts of the noise each maintain a variance of $\sigma^2/2$. In (1), x_p is the location, relative to scene center, in meters of the p^{th} target's scattering center; A_p symbolizes the complex-valued scattering coefficient of the p^{th} target; and α_p describes frequency dependence, i.e., scattering behavior, of the p^{th} target. The frequency dependence parameter, α, can take on a finite set of values for the specific geometries defined in Table 1. The scattering coefficient, $A = A_m e^{jA_\phi}$, can be represented by the magnitude and phase, A_m and A_ϕ, respectively. Previous research[43,44] presumed the parameter, A, in (1) was real-valued; i.e., targets behaved as perfect electrical conductors. Here, and in related works by authors of this manuscript, [45,46] that assumption is removed.

The 1-D electromagnetic scattering model in (1) represents the RF response of complex targets as a sum of contributions from canonical scattering components (e.g., dihedrals, flat plates, spheres, etc.), the properties of which are summarized by parameters, or features, which can be estimated from the measured signals. Estimation of these canonical target parameters from noisy radar signals represents a step within ATR algorithms in which target features are extracted (or estimated) and then subsequently used for target discrimination. An increased ability to correctly estimate target features when phase is retained, rather than discarded, will translate to improved ATR performance.

The 1-D electromagnetic scattering model in (1) was used for the derivation of novel CRLB expressions for target parameter estimation when phase is discarded.[45] A complex-valued 1-D radar range profile, or 1-D radar image, is generated through application of an inverse discrete Fourier transform (IDFT) to the collected phase history data. [49,50] The resulting imagery is modeled by a complex-valued Gaussian random variable, where the real and imaginary components of the complex signal are zero mean Gaussian random variables with identical variance. Therefore, the magnitude of the complex imagery is characterized by an uncorrelated Rician joint probability distribution function (pdf). [51,52] Both numerical and "approximate" expressions for the Rician CRLB were derived for target feature estimation error given 1-D radar range profiles.[45] The approximate Rician CRLB equations were shown to closely match the numerical solutions for all SNR, while requiring significantly fewer computations.[45]

5. FEATURE ESTIMATION RESULTS

Results of feature estimation simulations are presented in Figure 1, shown as target feature estimation error versus phase history domain SNR given noisy 1-D phase histories (Gaussian distributed) and 1-D radar range profiles (Rician distributed). CRLB curves report the square root of the CRLB, or the square root of the minimum achievable target estimation error variance. The impact of phase on the ability to correctly estimate target features from noisy signals is analyzed here with respect to various bandwidths. CRLB curves with respect to SNR are generated for cases when phase is retained (solid lines) and when it is discarded (dashed lines). Rician CRLB curves in these figures represent implementations of the

"approximate" expressions derived for 1-D magnitude imagery.[45] For all simulations, a center frequency, f_c, of 10 GHz is employed; thus, an X-band radar system is assumed.

It is assumed that all target parameters are unknown prior to estimation, including A_ϕ, which is not shown in Figure 1 since we cannot estimate it when phase is discarded. In addition, for a given 1-D phase history, a single stationary detected canonical target is assumed. This approach was chosen in order to identify if features of a single target could be accurately estimated when phase is discarded, i.e., a simple case in which the interference of multiple target returns is ignored. If results had shown that phase did not significantly assist in target parameter estimation, further investigation into more complicated target scene geometries would be futile. However, results do indeed demonstrate that frequency-dependent scattering characteristics, described by target parameter α, cannot be reliably estimated when phase is excluded.

Note that α maintains the set of values defined in Table 1. Possible values for the parameter α are therefore $[-1, -0.5, 0, 0.5, 1]$. Thus, the estimation error for this target feature must be less than 0.25 in order to distinguish a particular value of α from the next closest value of α. Figure 1c, offering CRLB curves for estimating α, also contains a solid black horizontal line designating a constant parameter estimation error of 0.25, across all SNR, to demonstrate data collection regions which allow for accurate estimation of α. Specifically, regions below this constant error line represent conditions under which α may be estimated from noisy data samples.

Target feature estimation accuracy results are shown in Figure 1. Bandwidths of 500 MHz, 1 GHz, 2 GHz and 6 GHz are simulated with a constant unambiguous range of 15 meters. The number of frequency samples, $N = [51, 101, 201, 601]$, changes with respect to bandwidths, BW = [500 MHz, 1 GHz, 2 GHz, 6 GHz], respectively, in order to maintain a constant unambiguous range or allowable scene size. For the results presented here, α maintains a value of zero, representative of the scattering from a spherical target. The scattering coefficient maintains values of 10.6 and 0 for its magnitude (A_m) and phase (A_ϕ), respectively. Therefore, for these experiments, the target exhibits PEC behavior. Figure 1 shows Rician and Gaussian CRLB curves for estimation of target parameters $\vec{\Theta} = [x, A_m, \alpha]$. CRLB curves increase in line thickness as bandwidth increases.

CRLB curves demonstrate that discarding phase does not significantly impact the ability to correctly estimate target position, x, or target scattering magnitude, A_m. Phase influences target parameter estimation accuracy more at low SNRs than high SNRs for target position and scattering magnitude. It is evident, however, that availability of phase information is imperative for estimation of the target frequency dependence parameter, α. Although an increase in bandwidth results in an increase in absolute parameter estimation accuracy, even with large bandwidths, α cannot be reliably estimated if phase is discarded. In other words, while α estimation error undoubtedly decreases as SNR and bandwidth increases, the ratio of the error when phase is excluded to the error achieved when phase is retained, does not change significantly with respect to SNR for a given bandwidth. This is seen by the nearly constant separation distance between pairs of Rician CRLB (dashed lines) and Gaussian CRLB (solid lines) curves for a particular bandwidth value. Note that for a 6 GHz bandwidth, the Rician CRLB curve crosses the solid black horizontal error line, i.e., the α estimation error is smaller than 0.25, at around 18 dB SNR. This suggests that given a 6 GHz bandwidth at X-band, classification techniques employing features for target discrimination may be able to distinguish between different target types with magnitude data within certain SNR ranges.

6. PHYSICAL SCATTERING MODELS FOR TARGET CLASSIFICATION

For target classification, we use physical scattering models of canonical scattering objects based on the geometrical theory of diffraction[47] that contain additional degrees of complexity compared to (1), such as the ability to specify the length, height and radius of the targets. Specifically, we will employ physics-based models for sphere, tophat and plate targets [53,54] for multinomial classification studies. While these models can be used to describe bistatic far-field scattering phenomenology, we assume the transmitter and receiver are co-located, i.e., a monostatic SAR collection geometry.[55] The general model for the received signal is given as[53]

$$S(f_n) = \sum_p \mathbf{P}_p M_{\Gamma(p)}(f_n, \theta, \phi; \vec{\Theta}_p) \exp(-j2\pi f_n \Delta R(\vec{\Theta}_p)/c) \tag{3}$$

where (θ, ϕ) denotes the azimuth and elevation angles, respectively. The function $M_{\Gamma(p)}$ characterizes the scattering response of the p^{th} target and $\mathbf{P}_p$ contains polarization information. The distance, $\Delta R(\vec{\Theta}_p)$, denotes the round-trip distance from the sensor to the p^{th} target, relative to the distance for a scatterer located at the scene center. This distance equivalently represents the range to the p^{th} target minus the range due to the target's curvature. Features describing the p^{th} target are

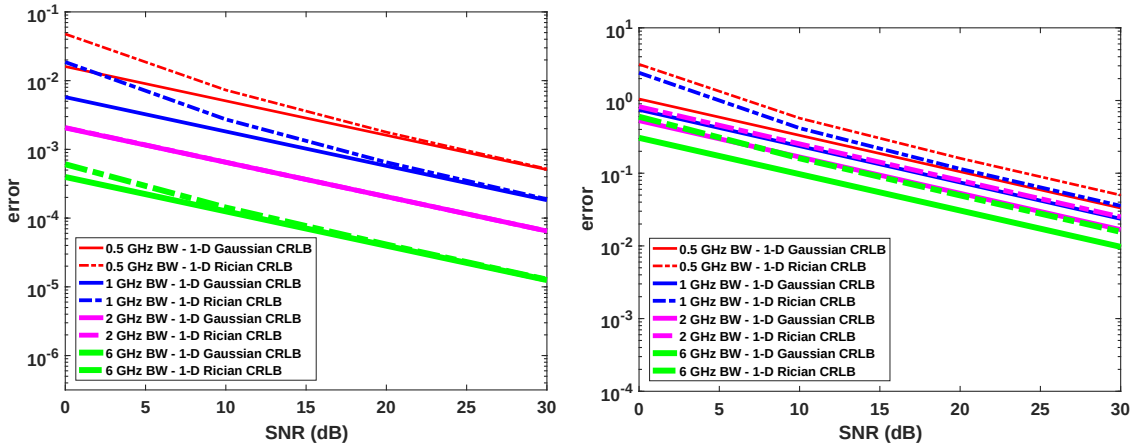

(a) Range Position (x)

(b) Scattering Magnitude (A_m)

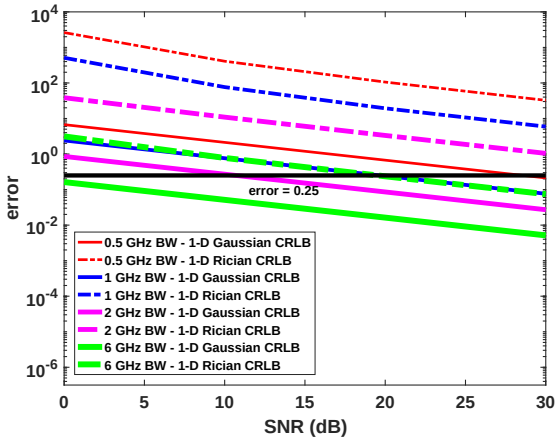

(c) Frequency Dependence (α)

Figure 1: 1-D Target Feature Estimation Error for Various Bandwidths and Constant Unambiguous Range. CRLB for bandwidths between 500 MHz and 6 GHz, with phase included (solid lines) or discarded (dashed lines), with respect to SNR, is shown. A 10 GHz center frequency and a 15 meter unambiguous range is assumed. Number of frequency samples employed increases with increasing bandwidths. Results are shown for (a) range position, (b) scattering magnitude, and (c) frequency dependence.

contained within $\vec{\Theta}$; these parameters include target location, orientation and size. The α parameter does not appear symbolically within these target scattering model expressions because equations are derived for individual target types and the corresponding α values are incorporated directly into the scattering equations. Note that in the referenced works, [53,54] θ denotes the elevation angle and ϕ denotes the azimuth angle. In this manuscript, we assume the opposite to be true in order to maintain consistency with the definition of θ as an azimuth angle in another publication. [46] The M_Γ and ΔR functions for a sphere are given as[53]

$$M_{\text{sphere}} = \sqrt{\pi} r \tag{4}$$

$$\Delta R^{\text{sphere}} = 2r \tag{5}$$

where r is the sphere radius. The M_Γ and ΔR functions for a tophat are given as[53]

$$M_{\text{tophat}} = H\sqrt{\frac{8r}{\sqrt{2}}}\sqrt{\frac{j2\pi f}{c}} \cdot \begin{cases} \sin(\phi), & \phi \in [0, \pi/4] \\ \cos(\phi), & \phi \in [\pi/4, \pi/2] \end{cases} \tag{6}$$

$$\Delta R^{\text{tophat}} = 2r\cos(\phi) \tag{7}$$

where r and H are the radius and height of the tophat, respectively. Finally, the M_Γ and ΔR functions for a plate are given as[53]

$$M_{\text{plate}} = \frac{j2\pi f LH}{c\sqrt{\pi}}(2\pi f L \sin\theta\cos\phi/c)(2\pi f H \sin\phi/c) \tag{8}$$

$$\Delta R^{\text{plate}} = 0 \tag{9}$$

where L and H are the length and height of the plate, respectively. An available software package that generates phase histories of canonical targets given these models was utilized for classification experimentation. [53,54]

7. LOGISTIC REGRESSION FOR MULTINOMIAL CLASSIFICATION

Logistic regression can be used to achieve multinomial classification through computation of posterior probabilities for C defined scatterer classes, labeled M_i, given a multi-dimensional feature vector, $\vec{x}$. Specifically, an assumption is made that the log-likelihood ratio for any pair of likelihoods within the scatterer classes can be represented as a linear combination of the feature values,[56]

$$\ln\left(\frac{p(\vec{x}|M_i)}{p(\vec{x}|M_C)}\right) = \beta_{i0} + \vec{\beta}_i^T\vec{x}, \qquad i = 1, ..., C-1 \tag{10}$$

where $\vec{\beta}_i$ is a vector of weights associated with scatterer class or model, M_i. The posterior probabilities can be thus described by the following,[56]

$$\begin{aligned} p(M_i|\vec{x}) &= \frac{\exp(\beta'_{i0} + \vec{\beta}_i^T\vec{x})}{1 + \sum_{i=1}^{C-1}\exp(\beta'_{i0} + \vec{\beta}_i^T\vec{x})}, \quad i = 1, ..., C-1 \\ p(M_C|\vec{x}) &= \frac{1}{1 + \sum_{i=1}^{C-1}\exp(\beta'_{i0} + \vec{\beta}_i^T\vec{x})} \end{aligned} \tag{11}$$

where $\beta'_{i0} = \beta_{i0} + \ln(p(M_i)/p(M_C))$.

A defined procedure for assigning a class label to an observed feature vector is called a decision rule, and for logistic discrimination, the decision rule relies solely on the previously defined linear functions of (11). The decision rule for this classifier states that we assign the observed feature set, $\vec{x}$, to class M_j if the following holds,[56]

$$\max\left\{\beta'_{i0} + \vec{\beta}_i^T\vec{x}\right\} = \beta'_{j0} + \vec{\beta}_j^T\vec{x} > 0, \quad i = 1, ..., C-1; \tag{12}$$

otherwise, we assign the observed feature set, $\vec{x}$, to class M_C. The weights associated with each scatterer class, $\vec{\beta}_i$, must be determined prior to execution of the decision rule. Note that knowledge of the class priors is not necessary, as seen in (11). The prior probabilities for the classes are folded into the weight values, specifically β'_{i0}, which will be directly estimated from the test data.

To obtain the maximum likelihood estimates of the β weights, we employ the Newton-Raphson method. [57] Values for β are chosen such that the log-likelihood function, $\mathcal{L}$, is maximized. For this logistic regression classification framework, the likelihood function of the observed features is given as [56]

$$\mathcal{L} = \prod_{i=1}^{C} \prod_{r=1}^{N_i} p(x_{ir}|M_i) \tag{13}$$

where $\vec{x}_{ir}(i = 1, 2, 3; r = 1, ..., N_i)$ represent the observations within class M_i for a three-class problem, such as the one we address in this manuscript. Since the features are assumed to be independent, and priors are included within the model weights, maximizing the likelihood functions is equivalent to maximizing the posterior probabilities. Therefore, the logarithm of an alternative likelihood function, $\mathcal{L}'$, is described by [56]

$$\ln(\mathcal{L}') = \sum_{i=1}^{C} \sum_{r=1}^{N_i} \ln(p(M_i|\vec{x}_{ir})) \tag{14}$$

and maximizing this function is equivalent to maximizing the likelihood function of (13). Finally, the derivatives of the log-likelihood function are computed for use by the Newton-Raphson method in generating maximum likelihood estimates of the model weights or parameters, β, [56]

$$\begin{aligned} \frac{\partial \ln(\mathcal{L}')}{\partial \beta'_{j0}} &= N_j - \sum_{\text{all } x} p(M_j|\vec{x}) \\ \frac{\partial \ln(\mathcal{L}')}{\partial (\beta_j)_l} &= \sum_{r=1}^{N_j} (x_{jr})_l - \sum_{\text{all } x} p(M_j|\vec{x}) x_l. \end{aligned} \tag{15}$$

An available software package that performs logistic regression classification was utilized for experiments performed here. [58]

8. TARGET FEATURE GENERATION FOR CLASSIFICATION STUDIES

Parametric scattering models of a sphere, tophat and plate that enable designation of the geometrical size attributes (height, length, radius, etc.) are employed for classification experiments. [53,54] These models were given in Section 6. Table 2 displays the specific parameters of the sphere, tophat and plate models used for the classification studies in this manuscript. A 10 GHz center frequency, f_c, and horizontal polarization (HH) is assumed for all classification experiments. In order to ensure the three scatterers are comparable from a signal power perspective, their sizes were chosen such that the magnitudes of the three scattering responses are identical at f_c. The magnitude at f_c was chosen to be 10.6 for all three target models. An azimuth angle of 0 degrees and an elevation angle of 5 degrees is assumed throughout. Note that the plate was rotated by 90 degrees in roll, and -5 degrees in pitch, to ensure its magnitude return at f_c matched that of the sphere and tophat given the target model and sensing geometry definitions. [53,54] Figures 2 and 4 provide 1-D phase history domain magnitude and phase profiles for the three models given bandwidths of 500 MHz and 6 GHz, respectively. These profiles provide some insight regarding the classification results described later throughout the text. Figures 3 and 5 provide 1-D image domain magnitude and phase profiles, formed via an inverse discrete Fourier transform, [49,50] for the three models given bandwidths of 500 MHz and 6 GHz, respectively. While features employed for classification studies in this manuscript are extracted directly from phase history domain data, Figures 3 and 5 indicate that phase information remains a source of target discrimination within the image domain. Note that the magnitude profiles in the image domain are nearly identical. The magnitude profiles in the phase history domain, as seen in Figures 2 and 4, are unique for each of the scattering models employed here, thus motivating the use of phase history domain feature sets.

Table 2: Canonical Model Parameters for Classification Studies

	sphere	tophat	plate
radius	6.0 m	0.3 m	-
height	-	6.5 m	0.3 m
length	-	-	0.3 m

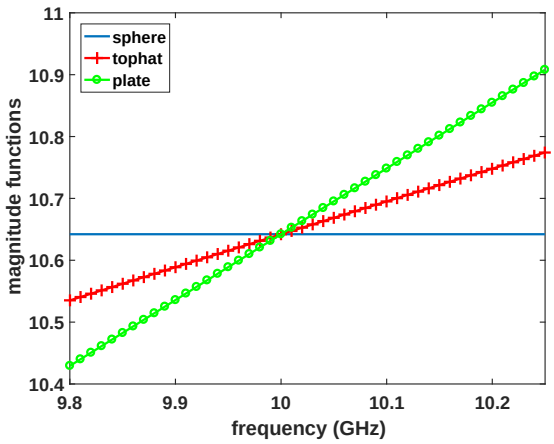

(a) Magnitude Profiles

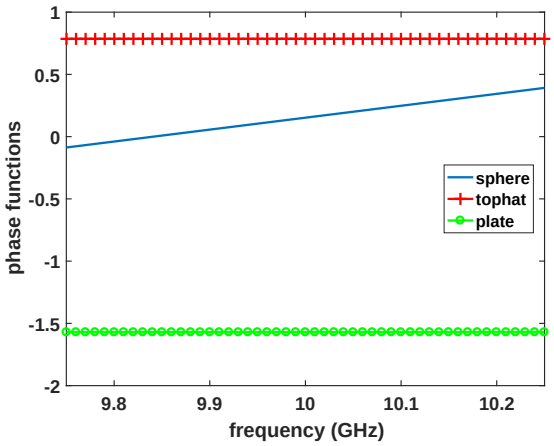

(b) Phase Profiles

Figure 2: Given three test targets (sphere, tophat and plate), the (a) magnitude and (b) phase profiles of the 1-D complex phase history are shown for a 500 MHz bandwidth and a 15 meter unambiguous range at X-band. Phase profiles represent unwrapped angular values in radians.

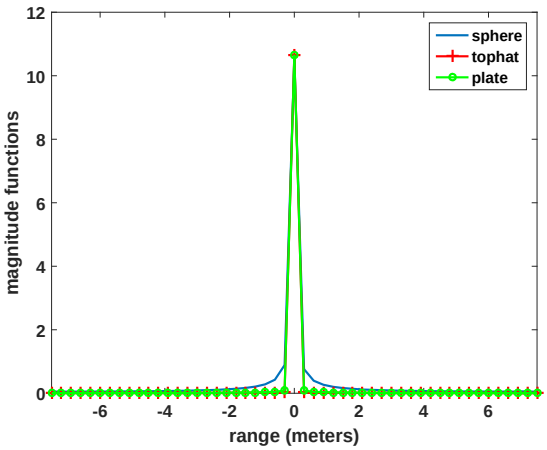

(a) Magnitude Profiles

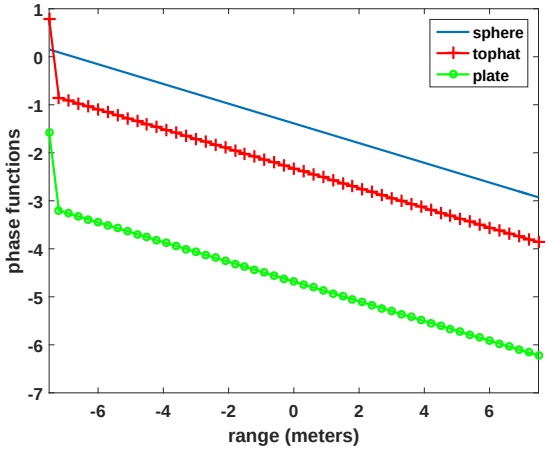

(b) Phase Profiles

Figure 3: Given three test targets (sphere, tophat and plate), the (a) magnitude and (b) phase profiles of the 1-D complex imagery (formed via inverse discrete Fourier transform) are shown for a 500 MHz bandwidth and a 15 meter unambiguous range at X-band. Phase profiles represent unwrapped angular values in radians.

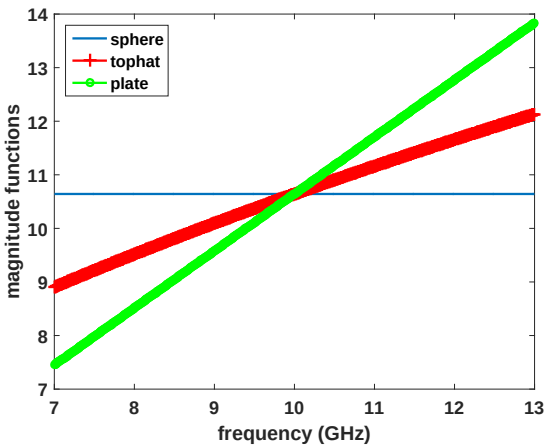

(a) Magnitude Profiles

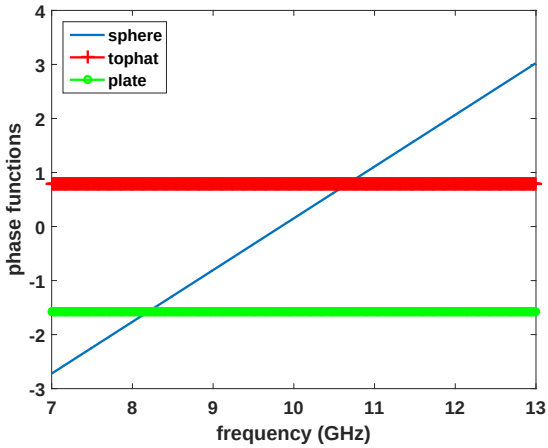

(b) Phase Profiles

Figure 4: Given three test targets (sphere, tophat and plate), the (a) magnitude and (b) phase profiles of the 1-D complex phase history are shown for a 6 GHz bandwidth and a 15 meter unambiguous range at X-band. Phase profiles represent unwrapped angular values in radians.

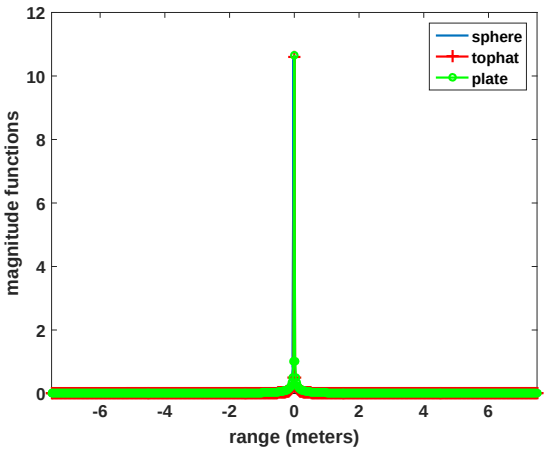

(a) Magnitude Profiles

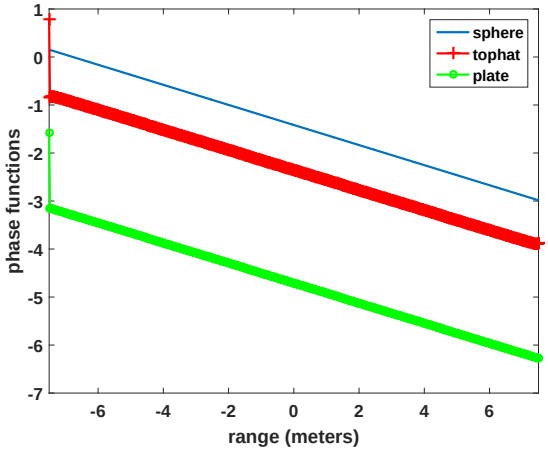

(b) Phase Profiles

Figure 5: Given three test targets (sphere, tophat and plate), the (a) magnitude and (b) phase profiles of the 1-D complex imagery (formed via inverse discrete Fourier transform) are shown for a 6 GHz bandwidth and a 15 meter unambiguous range at X-band. Phase profiles represent unwrapped angular values in radians.

We seek to quantify the impact of phase information with respect to radar scatterer classification for 1-D phase histories. Thus, we consider two different feature sets. The first is derived from complex radar responses and the second is derived from magnitude responses. In order to generate features from a set of noisy realizations, we first define complex templates and magnitude templates in the phase history domain. We choose to define these templates, and subsequently compute scatterer features, within the phase history domain since scattering characteristics are innately captured within this domain, rather than in the image domain, by an RF sensor. Note that while formed imagery may be beneficial for detection of a particular target within a scene, features of the target may be more distinctive within the domain in which they were sensed. The templates are bandwidth-dependent and vary in terms of the number of frequency samples. For all classification studies performed in this manuscript, a fixed unambiguous range of 15 meters is assumed; thus, the number of frequency samples, N, increases with increasing bandwidths. Assume the noiseless 1-D phase histories of the sphere, tophat and plate of Table 2 are denoted $S_{\text{sphere}}(f)$, $S_{\text{tophat}}(f)$ and $S_{\text{plate}}(f)$. The complex templates, or complex responses, are thus defined within a 3 x 1 vector,

$$\vec{t}_{\text{complex}} = \begin{bmatrix} S_{\text{sphere}}(f) \\ S_{\text{tophat}}(f) \\ S_{\text{plate}}(f) \end{bmatrix}. \tag{16}$$

Similarly, the magnitude templates, or magnitude responses, for the three models are defined within a 3 x 1 vector,

$$\vec{t}_{\text{magnitude}} = \begin{bmatrix} |S_{\text{sphere}}(f)| \\ |S_{\text{tophat}}(f)| \\ |S_{\text{plate}}(f)| \end{bmatrix}. \tag{17}$$

For a given SNR/bandwidth combination, 1000 Monte Carlo noisy realizations are produced from the original signatures for each of the three models, from which 1000 feature vectors are generated for each target class. Complex scatterer features are computed through calculation of the mean squared error (MSE) between each noisy realization for a given target class and each of the three complex templates. For example, given a fixed bandwidth and SNR, if the first complex noisy realization of the sphere model is denoted $\vec{\Psi}_1^{\text{sphere}}$, then the first complex feature vector (3 x 1) of this class is computed as follows,

$$\vec{\Lambda}_1^{\textbf{sphere}\ (\text{complex})} = \begin{bmatrix} \lambda_1^{\text{sphere}} \\ \lambda_1^{\text{tophat}} \\ \lambda_1^{\text{plate}} \end{bmatrix} = \begin{bmatrix} \frac{1}{N}\left(\vec{t}_{\text{complex}}(1) - \vec{\Psi}_1^{\textbf{sphere}}\right)^2 \\ \frac{1}{N}\left(\vec{t}_{\text{complex}}(2) - \vec{\Psi}_1^{\textbf{sphere}}\right)^2 \\ \frac{1}{N}\left(\vec{t}_{\text{complex}}(3) - \vec{\Psi}_1^{\textbf{sphere}}\right)^2 \end{bmatrix} \tag{18}$$

and similarly, the first magnitude feature vector (3 x 1) is computed as follows,

$$\vec{\Gamma}_1^{\textbf{sphere}\ (\text{magnitude})} = \begin{bmatrix} \gamma_1^{\text{sphere}} \\ \gamma_1^{\text{tophat}} \\ \gamma_1^{\text{plate}} \end{bmatrix} = \begin{bmatrix} \frac{1}{N}\left(\vec{t}_{\text{magnitude}}(1) - |\vec{\Psi}_1^{\textbf{sphere}}|\right)^2 \\ \frac{1}{N}\left(\vec{t}_{\text{magnitude}}(2) - |\vec{\Psi}_1^{\textbf{sphere}}|\right)^2 \\ \frac{1}{N}\left(\vec{t}_{\text{magnitude}}(3) - |\vec{\Psi}_1^{\textbf{sphere}}|\right)^2 \end{bmatrix}. \tag{19}$$

Thus, for a single classification experiment when phase is included, 1000 feature vectors are employed for each of the three target classes, given a particular bandwidth and SNR, as shown below.

$$\boldsymbol{\Lambda}^{\textbf{sphere}\ (\text{complex})} = \begin{bmatrix} \lambda_1^{\text{sphere}} & \lambda_2^{\text{sphere}} & \dots & \dots & \dots & \lambda_{999}^{\text{sphere}} & \lambda_{1000}^{\text{sphere}} \\ \lambda_1^{\text{tophat}} & \lambda_2^{\text{tophat}} & \dots & \dots & \dots & \lambda_{999}^{\text{tophat}} & \lambda_{1000}^{\text{tophat}} \\ \lambda_1^{\text{plate}} & \lambda_2^{\text{plate}} & \dots & \dots & \dots & \lambda_{999}^{\text{plate}} & \lambda_{1000}^{\text{plate}} \end{bmatrix} \tag{20}$$

$$\mathbf{\Lambda}^{\textbf{tophat}}\,(\text{complex}) = \begin{bmatrix} \lambda_1^{\text{sphere}} & \lambda_2^{\text{sphere}} & \cdots & \cdots & \cdots & \lambda_{999}^{\text{sphere}} & \lambda_{1000}^{\text{sphere}} \\ \lambda_1^{\text{tophat}} & \lambda_2^{\text{tophat}} & \cdots & \cdots & \cdots & \lambda_{999}^{\text{tophat}} & \lambda_{1000}^{\text{tophat}} \\ \lambda_1^{\text{plate}} & \lambda_2^{\text{plate}} & \cdots & \cdots & \cdots & \lambda_{999}^{\text{plate}} & \lambda_{1000}^{\text{plate}} \end{bmatrix} \tag{21}$$

$$\mathbf{\Lambda}^{\textbf{plate}}\,(\text{complex}) = \begin{bmatrix} \lambda_1^{\text{sphere}} & \lambda_2^{\text{sphere}} & \cdots & \cdots & \cdots & \lambda_{999}^{\text{sphere}} & \lambda_{1000}^{\text{sphere}} \\ \lambda_1^{\text{tophat}} & \lambda_2^{\text{tophat}} & \cdots & \cdots & \cdots & \lambda_{999}^{\text{tophat}} & \lambda_{1000}^{\text{tophat}} \\ \lambda_1^{\text{plate}} & \lambda_2^{\text{plate}} & \cdots & \cdots & \cdots & \lambda_{999}^{\text{plate}} & \lambda_{1000}^{\text{plate}} \end{bmatrix} \tag{22}$$

Likewise, for a single classification experiment in which phase is removed, the following three sets of scatterer features will be employed given a particular bandwidth and SNR.

$$\mathbf{\Gamma}^{\textbf{sphere}}\,(\text{magnitude}) = \begin{bmatrix} \gamma_1^{\text{sphere}} & \gamma_2^{\text{sphere}} & \cdots & \cdots & \cdots & \gamma_{999}^{\text{sphere}} & \gamma_{1000}^{\text{sphere}} \\ \gamma_1^{\text{tophat}} & \gamma_2^{\text{tophat}} & \cdots & \cdots & \cdots & \gamma_{999}^{\text{tophat}} & \gamma_{1000}^{\text{tophat}} \\ \gamma_1^{\text{plate}} & \gamma_2^{\text{plate}} & \cdots & \cdots & \cdots & \gamma_{999}^{\text{plate}} & \gamma_{1000}^{\text{plate}} \end{bmatrix} \tag{23}$$

$$\mathbf{\Gamma}^{\textbf{tophat}}\,(\text{magnitude}) = \begin{bmatrix} \gamma_1^{\text{sphere}} & \gamma_2^{\text{sphere}} & \cdots & \cdots & \cdots & \gamma_{999}^{\text{sphere}} & \gamma_{1000}^{\text{sphere}} \\ \gamma_1^{\text{tophat}} & \gamma_2^{\text{tophat}} & \cdots & \cdots & \cdots & \gamma_{999}^{\text{tophat}} & \gamma_{1000}^{\text{tophat}} \\ \gamma_1^{\text{plate}} & \gamma_2^{\text{plate}} & \cdots & \cdots & \cdots & \gamma_{999}^{\text{plate}} & \gamma_{1000}^{\text{plate}} \end{bmatrix} \tag{24}$$

$$\mathbf{\Gamma}^{\textbf{plate}}\,(\text{magnitude}) = \begin{bmatrix} \gamma_1^{\text{sphere}} & \gamma_2^{\text{sphere}} & \cdots & \cdots & \cdots & \gamma_{999}^{\text{sphere}} & \gamma_{1000}^{\text{sphere}} \\ \gamma_1^{\text{tophat}} & \gamma_2^{\text{tophat}} & \cdots & \cdots & \cdots & \gamma_{999}^{\text{tophat}} & \gamma_{1000}^{\text{tophat}} \\ \gamma_1^{\text{plate}} & \gamma_2^{\text{plate}} & \cdots & \cdots & \cdots & \gamma_{999}^{\text{plate}} & \gamma_{1000}^{\text{plate}} \end{bmatrix} \tag{25}$$

For the classification studies reported on in this manuscript, bandwidths between 500 MHz and 6 GHz are considered, in 500 MHz increments. SNRs between 0 and 30 dB are tested in 1 dB increments. Note that each of the three scatterers is represented by a data set which contains 1000 three-dimensional feature vectors for a particular SNR/bandwidth pair.

9. TARGET CLASSIFICATION RESULTS

We conduct an initial series of experiments where the target scattering coefficients are assumed to be real-valued. Figures 6 through 10 show the probability of correct classification as a function of phase history domain SNR for various bandwidths given the three scatterers (sphere, tophat and plate). Tables 3, 4 and 5 contain the probabilities of correct classification given the results reported in Figures 8, 9 and 10, respectively. An available software package that performs logistic regression classification was utilized for experiments performed here.[58]

Results of the simulations presented here validate the utility of phase information with respect to radar scatterer classification. Figures 6 and 7 provide curves of correct classification probability with and without phase for the three scatterers given a 500 MHz and 6 GHz bandwidth, respectively. Note that at a moderate bandwidth of 500 MHz, reliable discrimination between the scatterers is not possible for most SNRs considered when phase is discarded, as seen in Figure 6. In fact, the probability of correct classification is roughly 30% when phase is discarded for all three scatterers, at SNRs less than 15 dB, likening these classification decisions to a coin toss. Figure 7 demonstrates that as bandwidth increases, the classification rate when phase is discarded converges to the rate seen when phase is included.

Figures 8, 9 and 10 provide curves of correct classification rates with respect to phase history domain SNR when phase is either included or discarded for various bandwidths given the three targets. Bandwidths considered range from 500 MHz to 6 GHz with an incremental bandwidth value of 500 MHz. Line thickness increases with increasing bandwidth value; i.e., the thinnest line corresponds to a 500 MHz bandwidth while the thickest line corresponds to a bandwidth of 6 GHz. We observe that when phase is included, the probability of correct classification is nearly one for all SNRs and all bandwidths except the narrowest bandwidth under consideration, namely 500 MHz. Even in this case, the probability

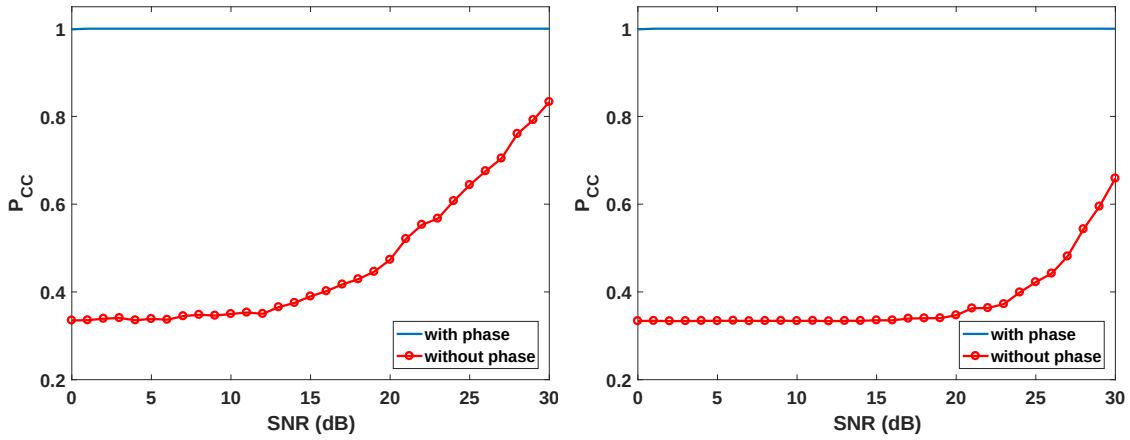

(a) Sphere

(b) Tophat

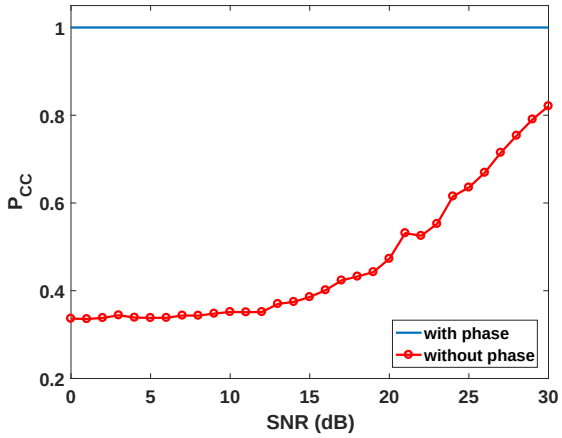

(c) Plate

Figure 6: Probability of Correct Classification via Logistic Regression for a 500 MHz Bandwidth. Results with simulated data are shown with respect to SNR when phase is either included or discarded for the (a) sphere, (b) tophat and (c) plate.

of correct classification at the lowest SNR is 0.99 or a 99% classification rate. When phase is excluded, the probability of correct classification will eventually converge to one at large SNR values. The rate of convergence of the probability of correct classification increases with increasing bandwidth values. The probabilities of correct classification for the three scatterers given real-valued scattering coefficients are summarized in Tables 3, 4 and 5. The ratio of the probability of correct classification when phase is included to that when phase is excluded is computed for each SNR/bandwidth pair. The average of these ratios across all SNRs for a given bandwidth is then reported in each of the tables as the rightmost column. Results suggest that phase information can improve scatterer classification by about a factor of 2.44 at low bandwidths. The impact of phase is less significant at higher bandwidths, with ratios of $1.03 - 1.21$ at a 6 GHz bandwidth for the three scatterers. Note that for a 6 GHz bandwidth, the probability of correct classification converges to one around 10 dB when phase is excluded, as demonstrated in Tables 3, 4 and 5.

10. CONCLUSIONS

This work first examined the impact of phase on the estimation of scatterer features within 1-D radar range profiles. A novel expression for the CRLB was employed for parameter estimates from magnitude imagery. Parameter estimation performance was considered for 1-D phase histories with respect to SNR and radar operating bandwidth. Phase information was shown to improve estimation accuracy of scatterer features described by electromagnetic scattering models. The most significant impact of discarding phase information was demonstrated in the decreased ability to accurately estimate

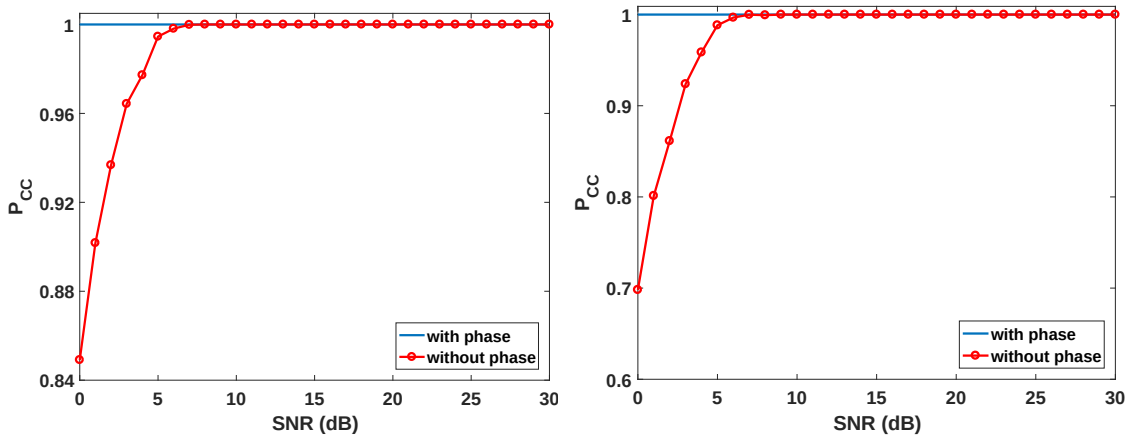

(a) Sphere (b) Tophat

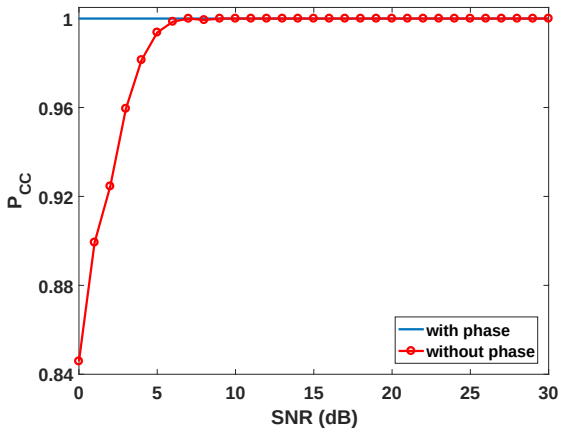

(c) Plate

Figure 7: Probability of Correct Classification via Logistic Regression for a 6 GHz Bandwidth. Results with simulated data are shown with respect to SNR when phase is either included or discarded for the (a) sphere, (b) tophat and (c) plate.

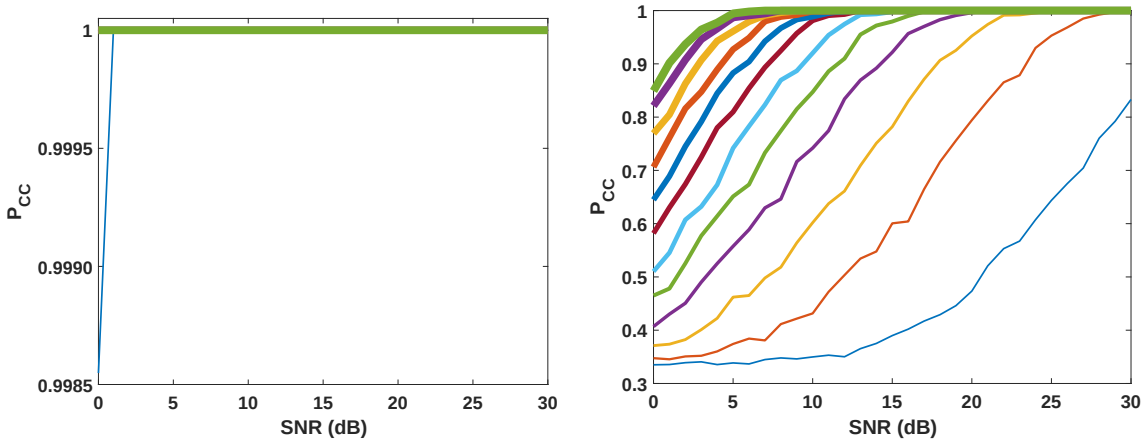

(a) With Phase (b) Without Phase

Figure 8: Probability of Correct Classification via Logistic Regression for a Sphere Given Various Bandwidths. Line thickness increases with increasing bandwidths from 500 MHz to 6 GHz at 500 MHz increments. Results with simulated data are shown with respect to SNR when phase is either (a) included or (b) discarded.

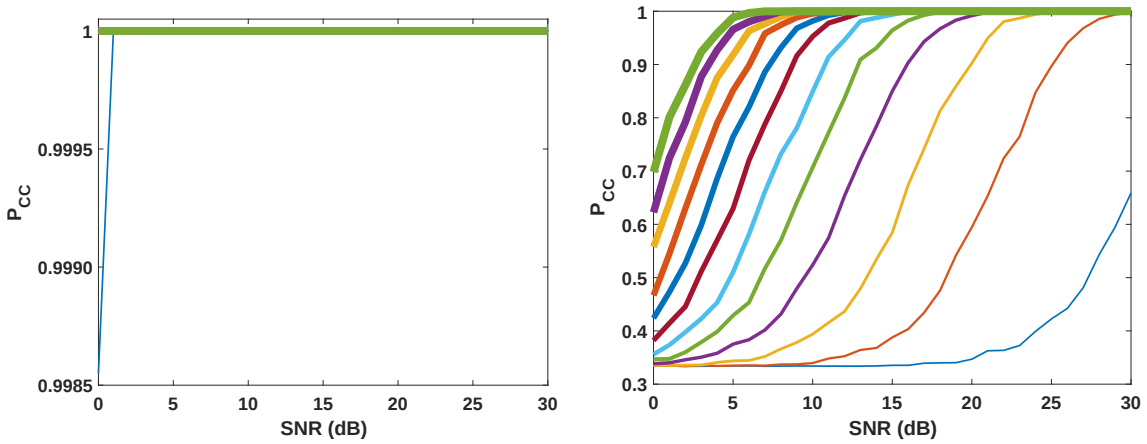

(a) With Phase (b) Without Phase

Figure 9: Probability of Correct Classification via Logistic Regression for a Tophat Given Various Bandwidths. Line thickness increases with increasing bandwidths from 500 MHz to 6 GHz at 500 MHz increments. Results with simulated data are shown with respect to SNR when phase is either (a) included or (b) discarded.

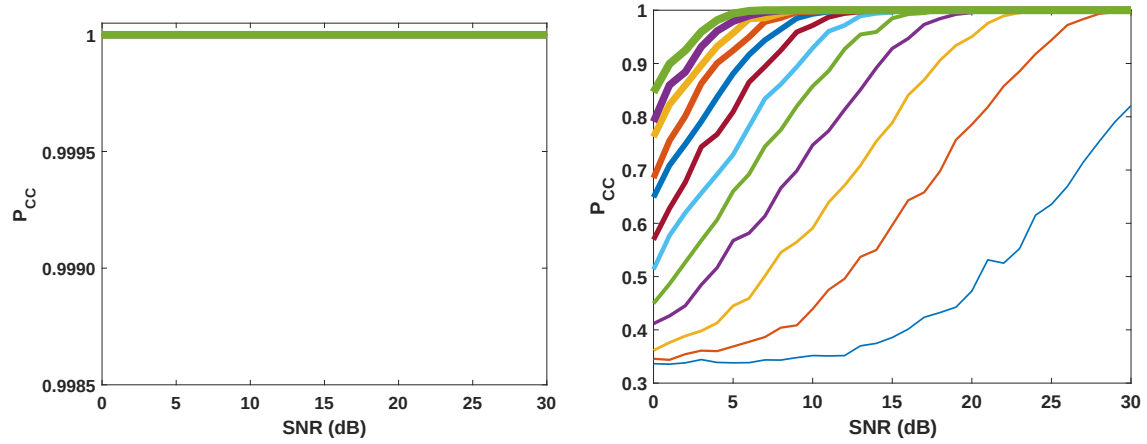

(a) With Phase (b) Without Phase

Figure 10: Probability of Correct Classification via Logistic Regression for a Plate Given Various Bandwidths. Line thickness increases with increasing bandwidths from 500 MHz to 6 GHz at 500 MHz increments. Results with simulated data are shown with respect to SNR when phase is either (a) included or (b) discarded.

Table 3: Probability of Correct Classification via Logistic Regression for a Sphere Given Various Bandwidths and Signal-to-Noise Ratios when Phase is Either Included (gray cells) or Discarded (white cells).

	0 dB		5 dB		10 dB		15 dB		20 dB		25 dB		30 dB		
	phase	no phase	phase	no phase	phase	no phase	phase	no phase	phase	no phase	phase	no phase	phase	no phase	Ave Ratio
500 MHz	0.999	0.335	1.000	0.339	1.000	0.350	1.000	0.390	1.000	0.473	1.000	0.644	1.000	0.833	2.318
1 GHz	1.000	0.348	1.000	0.374	1.000	0.432	1.000	0.601	1.000	0.794	1.000	0.953	1.000	0.999	1.835
1.5 GHz	1.000	0.371	1.000	0.462	1.000	0.602	1.000	0.782	1.000	0.952	1.000	0.999	1.000	1.000	1.550
2 GHz	1.000	0.407	1.000	0.558	1.000	0.742	1.000	0.922	1.000	0.996	1.000	1.000	1.000	1.000	1.384
2.5 GHz	1.000	0.465	1.000	0.651	1.000	0.847	1.000	0.979	1.000	1.000	1.000	1.000	1.000	1.000	1.270
3 GHz	1.000	0.510	1.000	0.742	1.000	0.920	1.000	0.998	1.000	1.000	1.000	1.000	1.000	1.000	1.200
3.5 GHz	1.000	0.582	1.000	0.810	1.000	0.981	1.000	1.000	1.000	1.000	1.000	1.000	1.000	1.000	1.139
4 GHz	1.000	0.645	1.000	0.883	1.000	0.989	1.000	1.000	1.000	1.000	1.000	1.000	1.000	1.000	1.099
4.5 GHz	1.000	0.706	1.000	0.927	1.000	0.999	1.000	1.000	1.000	1.000	1.000	1.000	1.000	1.000	1.071
5 GHz	1.000	0.769	1.000	0.961	1.000	1.000	1.000	1.000	1.000	1.000	1.000	1.000	1.000	1.000	1.049
5.5 GHz	1.000	0.821	1.000	0.987	1.000	1.000	1.000	1.000	1.000	1.000	1.000	1.000	1.000	1.000	1.033
6 GHz	1.000	0.849	1.000	0.995	1.000	1.000	1.000	1.000	1.000	1.000	1.000	1.000	1.000	1.000	1.026

Table 4: Probability of Correct Classification via Logistic Regression for a Tophat Given Various Bandwidths and Signal-to-Noise Ratios when Phase is Either Included (gray cells) or Discarded (white cells).

	0 dB		5 dB		10 dB		15 dB		20 dB		25 dB		30 dB		
	phase	no phase	phase	no phase	phase	no phase	phase	no phase	phase	no phase	phase	no phase	phase	no phase	Ave Ratio
500 MHz	0.999	0.334	1.000	0.334	1.000	0.334	1.000	0.335	1.000	0.347	1.000	0.422	1.000	0.659	2.441
1 GHz	1.000	0.334	1.000	0.335	1.000	0.340	1.000	0.388	1.000	0.595	1.000	0.897	1.000	0.997	2.016
1.5 GHz	1.000	0.335	1.000	0.344	1.000	0.394	1.000	0.584	1.000	0.903	1.000	0.999	1.000	1.000	1.875
2 GHz	1.000	0.339	1.000	0.375	1.000	0.524	1.000	0.850	1.000	0.992	1.000	1.000	1.000	1.000	1.770
2.5 GHz	1.000	0.347	1.000	0.429	1.000	0.707	1.000	0.964	1.000	1.000	1.000	1.000	1.000	1.000	1.656
3 GHz	1.000	0.356	1.000	0.510	1.000	0.849	1.000	0.994	1.000	1.000	1.000	1.000	1.000	1.000	1.563
3.5 GHz	1.000	0.382	1.000	0.630	1.000	0.953	1.000	1.000	1.000	1.000	1.000	1.000	1.000	1.000	1.465
4 GHz	1.000	0.424	1.000	0.765	1.000	0.982	1.000	1.000	1.000	1.000	1.000	1.000	1.000	1.000	1.384
4.5 GHz	1.000	0.467	1.000	0.852	1.000	0.996	1.000	1.000	1.000	1.000	1.000	1.000	1.000	1.000	1.332
5 GHz	1.000	0.557	1.000	0.918	1.000	1.000	1.000	1.000	1.000	1.000	1.000	1.000	1.000	1.000	1.269
5.5 GHz	1.000	0.622	1.000	0.966	1.000	1.000	1.000	1.000	1.000	1.000	1.000	1.000	1.000	1.000	1.235
6 GHz	1.000	0.698	1.000	0.988	1.000	1.000	1.000	1.000	1.000	1.000	1.000	1.000	1.000	1.000	1.206

Table 5: Probability of Correct Classification via Logistic Regression for a Plate Given Various Bandwidths and Signal-to-Noise Ratios when Phase is Either Included (gray cells) or Discarded (white cells).

	0 dB		5 dB		10 dB		15 dB		20 dB		25 dB		30 dB		
	phase	no phase	phase	no phase	phase	no phase	phase	no phase	phase	no phase	phase	no phase	phase	no phase	Ave Ratio
500 MHz	1.000	0.336	1.000	0.338	1.000	0.352	1.000	0.386	1.000	0.473	1.000	0.635	1.000	0.821	2.325
1 GHz	1.000	0.346	1.000	0.369	1.000	0.439	1.000	0.597	1.000	0.786	1.000	0.944	1.000	0.998	1.842
1.5 GHz	1.000	0.361	1.000	0.445	1.000	0.591	1.000	0.789	1.000	0.950	1.000	1.000	1.000	1.000	1.575
2 GHz	1.000	0.412	1.000	0.567	1.000	0.747	1.000	0.928	1.000	0.996	1.000	1.000	1.000	1.000	1.373
2.5 GHz	1.000	0.449	1.000	0.660	1.000	0.857	1.000	0.985	1.000	1.000	1.000	1.000	1.000	1.000	1.275
3 GHz	1.000	0.513	1.000	0.729	1.000	0.929	1.000	0.996	1.000	1.000	1.000	1.000	1.000	1.000	1.200
3.5 GHz	1.000	0.569	1.000	0.809	1.000	0.971	1.000	1.000	1.000	1.000	1.000	1.000	1.000	1.000	1.146
4 GHz	1.000	0.649	1.000	0.881	1.000	0.993	1.000	1.000	1.000	1.000	1.000	1.000	1.000	1.000	1.098
4.5 GHz	1.000	0.685	1.000	0.924	1.000	0.997	1.000	1.000	1.000	1.000	1.000	1.000	1.000	1.000	1.078
5 GHz	1.000	0.762	1.000	0.957	1.000	1.000	1.000	1.000	1.000	1.000	1.000	1.000	1.000	1.000	1.051
5.5 GHz	1.000	0.791	1.000	0.979	1.000	1.000	1.000	1.000	1.000	1.000	1.000	1.000	1.000	1.000	1.041
6 GHz	1.000	0.846	1.000	0.994	1.000	1.000	1.000	1.000	1.000	1.000	1.000	1.000	1.000	1.000	1.027

frequency-dependent scatterer curvature characteristics, i.e., the α parameter. Although an increase in bandwidth results in an increase in parameter estimation accuracy, even with large bandwidths, α cannot be reliably estimated if phase is discarded from 1-D radar range profiles.

In addition, we studied the impact of phase with respect to scatterer classification for simple canonical targets given features drawn from 1-D complex data and 1-D magnitude data. We chose fundamental scattering geometries in order to isolate the impact of phase information and to establish a theoretical foundation for future investigations into the use of radar phase in classification of more complex targets such as civilian vehicles. A logistic regression classifier was implemented to evaluate phase information in a principled manner. This classifier made no assumptions on the underlying distribution of the data, although the features were considered independent. Inclusion of radar phase resulted in improved performance in classification rates. Correct classification rates were roughly $1.03 - 2.44$ times better when phase was retained rather than discarded, with larger improvement gains seen at low bandwidths and low SNRs. Phase was shown to enable discrimination between targets that have similar magnitude profiles in the image domain when correct classification of the targets was not possible with magnitude data.

11. FUTURE WORK

A suggested approach to determining the usefulness of phase in radar ATR applications is to incrementally increase the complexity of the problem so as to isolate the significance of each contributing factor. A natural extension of the work presented here would be the consideration of nearby stationary canonical scatterers in a scene. Specifically, a meaningful research avenue is the investigation of the impact of phase on scatterer feature extraction and/or classification when the returns from neighboring scatterers interfere with the observed response of the scatterer of interest. Additional research involves examining information in phase given more complex stationary targets, e.g., civilian vehicles, as it relates to the ability to perform reliable target recognition. Such an extension of the work presented here would exploit the characteristics of high frequency radar scattering, described by the geometrical theory of diffraction, which allows the return of a complex target to be represented as a sum of the returns of individual canonical scattering elements. Finally, an additional research area of interest involves examining the impact of phase when classifying moving targets. If the additional degree of

complexity of movement is introduced, it is suggested that the analysis begins with simple canonical scatterers that are moving and progresses to more sophisticated moving targets in a manner similar to that described here for stationary target analysis. In summary, preserving and processing all measured information may not be practical in all situations. The sheer volume of collected data may be a limiting factor for some applications, such as persistent surveillance. However, a thorough understanding of the cost of a reduction in data with respect to radar target classification is imperative and serves as a motivation for the work presented within this manuscript.

ACKNOWLEDGMENTS

The authors would like to thank the National Science Foundation, the Dayton Area Graduate Studies Institute, and the Air Force Research Laboratory for their very much appreciated financial support throughout the pursuit of this research.

REFERENCES

[1] Datcu, M., Schwarz, G., Soccorsi, M., and Chaabouni, H., "Phase information contained in meter-scale SAR images," in [*Remote Sensing*], 67460H–67460H, International Society for Optics and Photonics (2007).

[2] El-Darymli, K., McGuire, P., Power, D., and Moloney, C., "Rethinking the phase in single-channel SAR imagery," in [*2013 14th International Radar Symposium (IRS)*], **1**, 429–436, IEEE (2013).

[3] Samu, T. I., Sadjadi, F. A., and Hall, E. L., "Three-dimensional moment invariants for automated target recognition," in [*Automatic Object Recognition VI*], Sadjadi, F. A., ed., *Proc. SPIE* **2756**, 230–237 (1996).

[4] Ross, T. D., Bradley, J. J., Hudson, L. J., and O'Connor, M. P., "SAR ATR - So What's The Problem? An MSTAR Perspective," in [*Algorithms for Synthetic Aperture Radar Imagery VI*], Zelnio, E. G. and Garber, F. D., eds., *Proc. SPIE* **3721**, 662–672 (1999).

[5] Ross, T. D. and Goodwon, L. C., "Improved Automatic Target Recognition (ATR) Value Through Enhancements and Accommodations," in [*Algorithms for Synthetic Aperture Radar Imagery XIII*], Zelnio, E. G. and Garber, F. D., eds., *Proc. SPIE* **6237** (2006).

[6] Ross, T., "ATR Theory Issues," in [*Algorithms for Synthetic Aperture Radar Imagery XI*], Zelnio, E. G. and Garber, F. D., eds., *Proc. SPIE* **5427**, 459–470 (2004).

[7] Dudgeon, D. E., "ATR performance modeling and estimation," in [*Technical Report 1051*], Massachusetts Institute of Technology Lincoln Laboratory (December 1998).

[8] Fisher III, J. W. and Willsky, A. S., "Information theoretic feature extraction for ATR," in [*Conference Record of the Thirty-Third Asilomar Conference on Signals, Systems, and Computers*], **2**, 1245–1249, IEEE (1999).

[9] Blacknell, D., "Feature analysis for SAR ATR," in [*SAR Image Analysis, Modeling, and Techniques III*], Posa, F. and Guerriero, L., eds., *Proc. SPIE* **4173**, 75–86 (2000).

[10] Chamberlain, N. E., Walton, E. K., and Garber, F. D., "Radar target identification of aircraft using polarization-diverse features," *Aerospace and Electronic Systems, IEEE Transactions on* **27**(1), 58–67 (1991).

[11] Snorrason, O. and Garber, F. D., "Evaluation of nonparametric discriminant analysis techniques for radar signal feature selection and extraction," *Optical Engineering* **31**(12), 2608–2617 (1992).

[12] Fogler, R. J., Koch, M. W., Moya, M. M., and Hush, D. R., "Feature discovery on segmented objects in SAR imagery using self-organizing neural networks," in [*Applications of Artificial Neural Networks IV*], Rogers, S. K., ed., *Proc. SPIE* **1965**, 209–220 (1993).

[13] Yu, X., Hoff, L. E., Reed, I. S., Buck, D. L., and Chen, A. M., "Comparative study of feature mapping and selection for ATR: experiments on SAR data," in [*Algorithms for Synthetic Aperture Radar Imagery*], Giglio, D. A., ed., *Proc. SPIE* **2230**, 275–284 (1994).

[14] Shunping, X., Xuesong, W., Yonghu, Z., Huamin, T., Zhaowen, Z., and Guirong, G., "Feature-extracting and recognition based on radar target's dynamic polarization structure," in [*Proceedings, CIE International Conference of Radar*], 666–670, IEEE (1996).

[15] Chiang, H.-C., Moses, R. L., and Potter, L. C., "Model-based classification of radar images," *Information Theory, IEEE Transactions on* **46**(5), 1842–1854 (2000).

[16] Principe, J. C., Xu, D., Zhao, Q., and Fisher III, J. W., "Learning from examples with information theoretic criteria," *Journal of VLSI Signal Processing Systems for Signal, Image and Video Technology* **26**(1), 61–77 (2000).

[17] Xu, J., Yang, J., and Peng, Y.-N., "New method of feature extraction in polarimetric SAR image classification," in [*Battlespace Digitization and Network-Centric Warfare II*], Suresh, R. and Roper, W. E., eds., *Proc. SPIE* **4741**, 337–344 (2002).

[18] Zhang, G., Hu, L., and Jin, W., "Complexity feature extraction of radar emitter signals," in [*Proceedings, Asia-Pacific Conference on Environmental Electromagnetics, 2003 (CEEM 2003)*], 495–498, IEEE (2003).

[19] Zhang, J., Song, R., Yu, W., Xia, S., and Hu, W., "Visual effects based feature extraction for dynamic radar target echo series," in [*Proceedings, 7th International Conference on Signal Processing*], **3**, 2111–2115, IEEE (2004).

[20] Choi, I.-S. and Kim, H.-T., "Feature extraction of radar targets using Evolutionary Adaptive Wavelet Transform," in [*2007 Korea-Japan Microwave Conference (KJMW 2007)*], 129–132, IEEE (2007).

[21] Sun, Y., Xue, M., Li, J., and Stanfill, S. R., "Improving ATR performance through distance metric learning," in [*Algorithms for Synthetic Aperture Radar Imagery XIV*], Zelnio, E. G. and Garber, F. D., eds., *Proc. SPIE* **6568** (2007).

[22] Zhu, F., Zhang, X.-D., Hu, Y.-F., and Xie, D., "Nonstationary hidden Markov models for multiaspect discriminative feature extraction from radar targets," *Signal Processing, IEEE Transactions on* **55**(5), 2203–2214 (2007).

[23] Chen, T., Jin, W., and Chen, Z., "Feature extraction using wavelet transform for radar emitter signals," in [*WRI International Conference on Communications and Mobile Computing (CMC 2009)*], **1**, 414–418, IEEE (2009).

[24] Stausberger, D., Garber, E., Chamberlain, N., and Walton, E. K., "Modeling and performance of HF/OTH radar target classification systems," *IEEE Transactions on Aerospace and Electronic Systems* **28**(2), 396–403 (1992).

[25] Zhai, Y., Li, J., Guo, C., and Xu, Y., "SAR automatic target recognition based on Local Phase Quantization plus Biomimetic Pattern Recognition," in [*Signal Processing (ICSP), 2012 IEEE 11th International Conference on*], **3**, 1885–1889, IEEE (2012).

[26] Dong, G., Kuang, G., Zhao, L., Lu, J., and Lu, M., "Joint sparse representation of monogenic components: With application to automatic target recognition in SAR imagery," in [*2014 IEEE Geoscience and Remote Sensing Symposium*], 549–552, IEEE (2014).

[27] El-Darymli, K., Mcguire, P., Gill, E. W., Power, D., and Moloney, C., "Holism-based features for target classification in focused and complex-valued synthetic aperture radar imagery," *IEEE Transactions on Aerospace and Electronic Systems* **52**(2), 786–808 (2016).

[28] Rihaczek, A. W., "Radar resolution of ideal point scatteerers," *IEEE Transactions on Aerospace and Electronic Systems* **32**(2), 842–845 (1996).

[29] Rihaczek, A. and Hershkowitz, S., "Man-made target backscattering behavior: applicability of conventional radar resolution theory," *IEEE Transactions on Aerospace and Electronic Systems* **32**(2), 809–824 (1996).

[30] El-Darymli, K., Moloney, C., Gill, E., McGuire, P., and Power, D., "Recognition of nonlinear dispersive scattering in SAR imagery," in [*2014 IEEE Geoscience and Remote Sensing Symposium*], 4722–4725 (July 2014).

[31] Ma, J. and Ahalt, S. C., "Complex HRR range signatures," in [*Targets and Backgrounds VI: Characterization, Visualization, and the Detection Process*], Watkins, W. R., Clement, D., and Reynolds, W. R., eds., *Proc. SPIE* **4029**, 130–135 (2000).

[32] Zelnio, A. M., Moore, L. J., Roush, C. R., and Rigling, B. D., "Cramér-Rao lower bound on time of arrival estimates for an envelope-detected pulse," in [*Radar Conference (RADAR), 2013 IEEE*], 1–4, IEEE (2013).

[33] Lin, Y.-T. and Ksienski, A., "Identification of complex geometrical shapes by means of low-frequency radar returns," *Radio and Electronic Engineer* **46**(10), 472–486 (1976).

[34] Wenli, J., Haifeng, J., Zhiwen, L., and Youan, K., "Study on radar range profiles for target recognition," in [*Radar, 1996. Proceedings., CIE International Conference of*], 648–652 (Oct 1996).

[35] Du, L., Liu, H., and Bao, Z., "Radar automatic target recognition based on complex high-resolution range profiles," in [*2006 CIE International Conference on Radar*], 1–5, IEEE (2006).

[36] Du, L., Liu, H., Bao, Z., and Zhang, J., "Radar automatic target recognition using complex high-resolution range profiles," *IET Radar, Sonar & Navigation* **1**(1), 18–26 (2007).

[37] Chen, L. and Chen, R., "A new radar target recognition method based on complex high resolution range profiles," in [*Microwave and Millimeter Wave Technology (ICMMT), 2012 International Conference on*], **2**, 1–4, IEEE (2012).

[38] Mikhnev, V., Badeev, V., and Vainikainen, P., "Microwave visualization of layered dielectric half-space using range profiling of phase," in [*11th International Radar Symposium*], 1–4, IEEE (2010).

[39] Mikhnev, V. and Vainikainen, P., "Experimental studies of subsurface target discrimination using a phase-based microwave imaging method," in [*Advanced Ground Penetrating Radar (IWAGPR), 2011 6th International Workshop on*], 1–4, IEEE (2011).
[40] Sadjadi, F. A., "Classification of polarimetric radar signatures using scatterers' joint amplitude and phase distribution functions," in [*AeroSense 2003*], 290–300, International Society for Optics and Photonics (2003).
[41] Malas, J., Pasala, K. M., et al., "Information theory based radar signature analysis," in [*Aerospace Conference, 2007 IEEE*], 1–13, IEEE (2007).
[42] Malas, J., Pasala, K. M., et al., "Radar signature analysis using information theory," in [*Radar Conference, 2008. RADAR'08. IEEE*], 1–6, IEEE (2008).
[43] Rigling, B., Potter, L. C., and Moses, R. L., "Relative information in phase of radar range profiles," in [*Algorithms for Synthetic Aperture Radar Imagery VII*], *Proc. SPIE* **4053**, 211–218 (2000).
[44] Rigling, B., *Physics, Fisher, and Phase: Information Content in SAR Images*, Master's thesis, The Ohio State University (2000).
[45] Moore, L., Rigling, B., and Penno, R., "Characterization of information in phase of radar range profiles," in [*Signals, Systems and Computers, 2014 48th Asilomar Conference on*], 2027–2031 (Nov 2014).
[46] Moore, L. J., *Impact of Phase Information on Radar Automatic Target Recognition*, PhD thesis, University of Dayton (2016).
[47] Keller, J. B., "Geometrical theory of diffraction," *JOSA* **52**(2), 116–130 (1962).
[48] Potter, L. C., Chiang, D.-M., Carriere, R., and Gerry, M. J., "A GTD-based parametric model for radar scattering," *Antennas and Propagation, IEEE Transactions on* **43**(10), 1058–1067 (1995).
[49] Jakowatz, C., Wahl, D., Eichel, P., Ghiglia, D., and Thompson, P., [*Spotlight-Mode Synthetic Aperture Radar: A Signal Processing Approach*], Kluwer Academic Publishers, USA (1999).
[50] Gorham, L. A. and Moore, L. J., "SAR image formation toolbox for MATLAB," in [*Algorithms for Synthetic Aperture Radar Imagery XVII*], Zelnio, E. G. and Garber, F. D., eds., *Proc. SPIE* **7699**, 769906 (2010).
[51] Papoulis, A. and Pillai, S. U., [*Probability, random variables, and stochastic processes*], Tata McGraw-Hill Education (2002).
[52] Beaulieu, N. C. and Hemachandra, K. T., "Novel simple forms for multivariate Rayleigh and Rician distributions with generalized correlation," in [*2010 IEEE Global Telecommunications Conference GLOBECOM 2010*], (2010).
[53] Jackson, J. A., Rigling, B. D., and Moses, R. L., "Parametric scattering models for bistatic synthetic aperture radar," in [*2008 IEEE Radar Conference*], 1–5, IEEE (2008).
[54] Jackson, J. A., Rigling, B. D., and Moses, R. L., "Canonical scattering feature models for 3D and bistatic SAR," *IEEE Transactions on Aerospace and Electronic Systems* **46**(2), 525–541 (2010).
[55] Sullivan, R. J., [*Radar Foundations for Imaging and Advanced Concepts*], SciTech Publishing, Inc., Raleigh, NC (2004).
[56] Webb, A. R., [*Statistical pattern recognition*], John Wiley & Sons (2003).
[57] Hasselblad, V., "Estimation of parameters for a mixture of normal distributions," *Technometrics* **8**(3), 431–444 (1966).
[58] Chen, M., [*Logistic Regression for Classification Software Package*], Matlab File Exchange (2016).